



Research paper

Novel 6-substituted benzoyl and non-benzoyl straight chain pyrrolo [2,3-*d*]pyrimidines as potential antitumor agents with multitargeted inhibition of TS, GARFTase and AICARFTase



Ruijuan Xing^{a,1}, Hongying Zhang^{a,1}, Jiansong Yuan^a, Kai Zhang^a, Lin Li^a, Huicai Guo^b, Lijuan Zhao^b, Congying Zhang^a, Shuolei Li^a, Tianfeng Gao^a, Yi Liu^{b,*}, Lei Wang^{a,**}

^a Department of Medicinal Chemistry, School of Pharmacy, Hebei Medical University, Shijiazhuang 050017, China

^b Department of Toxicology, School of Public Health, Hebei Medical University, Shijiazhuang 050017, China

ARTICLE INFO

Article history:

Received 15 December 2016

Received in revised form

25 March 2017

Accepted 11 August 2017

Available online 14 August 2017

Keywords:

pyrrolo[2,3-*d*]pyrimidines

Antiproliferation

Multitargeted inhibition

Cell cycle arrest

Apoptosis

ABSTRACT

A novel series of 6-substituted benzoyl and non-benzoyl straight chain pyrrolo[2,3-*d*]pyrimidines were designed and synthesized as potential antitumor agents targeting both thymidylate and purine nucleotide biosynthesis. Starting from the key intermediate 2-amino-4-oxo-pyrrolo[2,3-*d*]pyrimidin-6-yl-acetic acid, target compounds **1–6** were successfully obtained through two sequential condensation and saponification reactions in decent yield. The newly synthesized compounds showed antiproliferative potencies against a panel of tumor cell lines including KB, SW620 and MCF7. In particular, most compounds of this series exhibited nanomolar to subnanomolar inhibitory activities toward KB tumor cells, significantly more potent than the positive control methotrexate (MTX) and pemetrexed (PMX). Along with the results of nucleoside protection assays, molecular modeling studies suggested that the antitumor activity of compound **6** could be attributed to multitargeted inhibition of folate-dependent enzymes thymidylate synthase (TS), glycinamide ribonucleotide formyltransferase (GARFTase) and 5-aminoimidazole-4-carboxamide ribonucleotide formyltransferase (AICARFTase). Growth inhibition by compound **6** also induced distinct early apoptosis and cell cycle arrest at S-phase, which resulted in cell death.

© 2017 Elsevier Masson SAS. All rights reserved.

1. Introduction

Classical antifolates, analogs of folic acid, were among the first effective chemotherapeutic agents and were clinically used as antimicrobial, antifungal, antiinflammatory and antitumor agents [1–3]. Dihydrofolate reductase (DHFR) and thymidylate synthase (TS) are two main intracellular targets of antifolates [4–7], albeit several other important enzymes are involved in the folate cycle. DHFR catalyzes the reduction of folic acid to dihydrofolate which was further reduced to active folate, tetrahydrofolate (THF), as one carbon carrier that donates methyl groups to end target molecules [8]. TS, however, functions as a catalyst for the de novo biosynthesis

of thymidine monophosphate (dTMP) from deoxyuridine monophosphate (dUMP) [9]. Inhibition of DHFR results in partial depletion of intracellular reduced folates, causing cells incapable of undergoing accurate DNA replication, ultimately leading to cell death [8]. TS inhibition leads to so called “thymineless state”, in which cells experience starvation of thymidine triphosphate (dTTP) and undergo irreversible cell death [9]. The most commonly used DHFR inhibitor is methotrexate (MTX, Fig. 1) [10], which binds to DHFR reversibly and impedes its function by decreasing supplies of thymidine and purine bases for DNA and RNA synthesis. Another representative DHFR inhibitor is pralatrexate (PDX, Fig. 1) [11,12], which was approved in 2009 as a chemotherapy of relapsed or refractory peripheral T-cell lymphoma. Structurally, a 2,4-diaminopyrimidine moiety is required for binding to the active sites of DHFR. TS inhibitors, however, have a 2-amino-4-oxo-pyrimidine part in their scaffolds as in pemetrexed (PMX, Fig. 1) [13], or a 2-methyl-4-oxo-pyrimidine moiety as in raltitrexed (RTX, Fig. 1) [14].

* Corresponding author.

** Corresponding author.

E-mail addresses: liuyi78@hebmu.edu.cn (Y. Liu), hmuwanglei@hebmu.edu.cn (L. Wang).

¹ Equally contributed to this work.

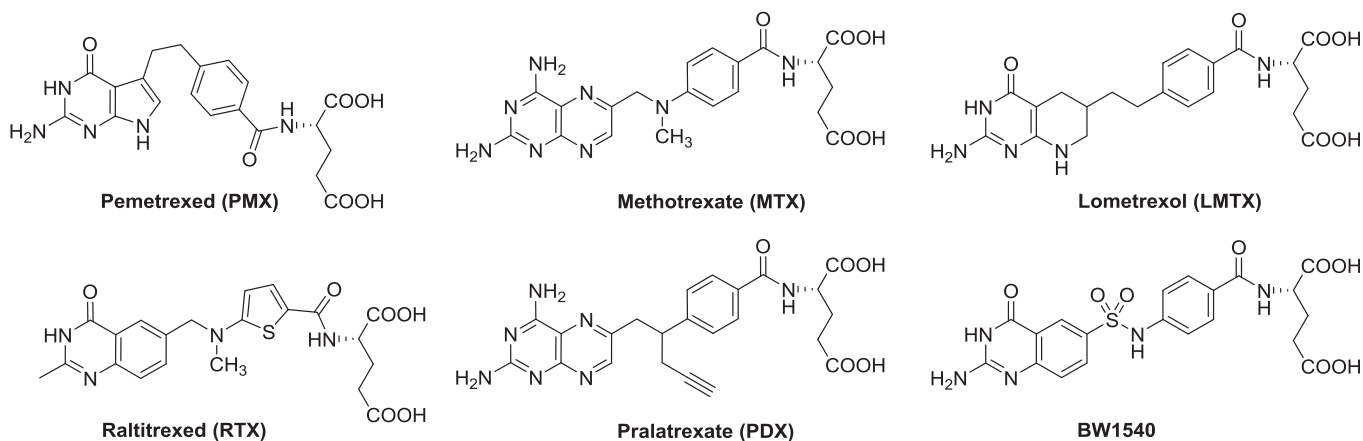


Fig. 1. Structures of classical antifolates.

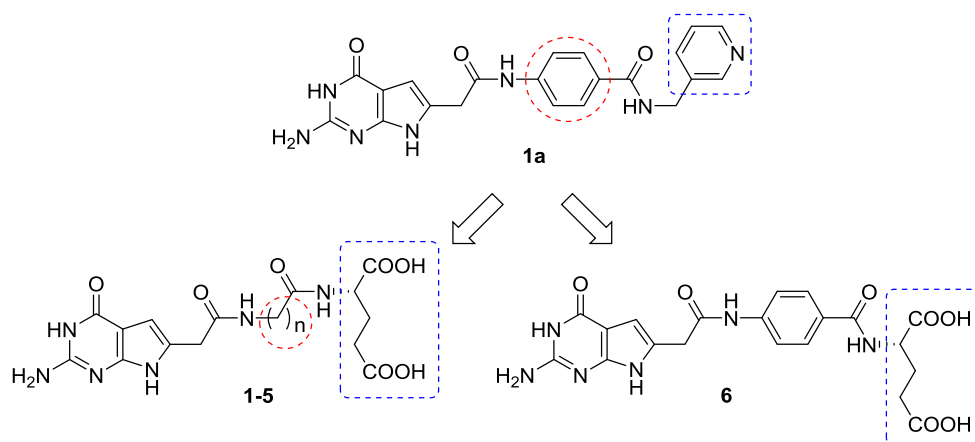


Fig. 2. Design of 6-substituted pyrrolo[2,3-d]pyrimidines 1–6.

The two folate-dependent enzymes glycinamide ribonucleotide formyltransferase (GARFTase) and 5-aminoimidazole-4-carboxamide ribonucleotide formyltransferase (AICARFTase) were also considered as intracellular targets of antifolates. GARFTase catalyzes the incorporation of C-8 into inosine monophosphate (IMP) by transferring the formyl group from N^{10} -formyl-tetrahydrofolate (N^{10} -formyl-THF) to the side-chain amino group of glycinamide ribonucleotide (GAR) to produce formylglycinamide ribonucleotide (FGAR) and THF [15,16]. AICARFTase, however, catalyzes the formation of C-2 of IMP through transferring the formyl group from N^{10} -formyl-THF to 5-amino group of 5-aminoimidazole-4-carboxamide ribonucleotide (AICAR) to yield 5-formylaminoimidazole-4-carboxamide ribonucleotide (FAICAR) [16,17].

Compared with the number of DHFR or TS inhibitors used in clinics, specific inhibitors of GARFTase or AICARFTase have been scarce. Lometrexol (LMTX, Fig. 1) [18,19], the first GARFTase inhibitor to enter clinical trials, was abandoned eventually due to severe and cumulative myelosuppression and mucositis in phase I clinical trials. BW1540 (Fig. 1) [20], a sulfamido-bridged 5,8-dideazafolate analog with potent inhibition of AICARFTase ($K_i = 8$ nM), was not taken into clinical trials yet.

Drug resistance is easily developed for antifolates with specific inhibition of only one folate-dependent enzyme. As an exception, PMX, originally considered as a specific TS inhibitor, is actually a

multitargeted agent against TS, DHFR, GARFTase and AICARFTase [21,22]. Thus, multitargeted antifolates would seem to have substantial advantages over mono-targeted antifolates when tumors become resistant due to alterations in one or the other targeted enzyme. In our previous studies [23,24], we designed and synthesized a series of multitargeted antifolates with a pyrrolo[2,3-d]pyrimidine core structure (1a, Fig. 2). These compounds showed potent antiproliferative activities against several tumor cell lines including KB, A549 and HepG2, while the intracellular targets were identified as TS, GARFTase and AICARFTase. Our interest is to develop novel multitargeted antifolates as antitumor agents and to optimize the structures for better inhibition of folate metabolizing enzymes than PMX. In this study, the side chain pyridyl-3-methylamino group of the lead compound 1a (Fig. 2) was replaced by a glutamate to provide target compound 6 (Fig. 2) as a classical analog. This isosteric replacement would enable 6 to undergo polyglutamylation at the γ -carboxyl moiety by the enzyme folypoly- γ -glutamate synthetase (FPGS) [25], resulting in increased binding to target enzymes at low concentrations and intracellular retention through metabolic trapping. The non-benzoyl straight chain analogs 1–5 (Fig. 2) were also designed and synthesized to explore the importance of the side chain phenyl ring for antitumor activity, as well as the optimal distance of the alkyl amide linker between the core structure of pyrrolo[2,3-d]pyrimidine and the γ -glutamate moiety.

2. Chemistry

Target compounds **1–6** were synthesized as shown in [Scheme 1](#) and [Scheme 2](#). The key intermediate 2-amino-4-oxo-pyrrolo[2,3-*d*]pyrimidin-6-yl-acetic acid, **10**, was obtained by a condensation reaction of 2,4-diamino-6-hydroxypyrimidine, **7**, and ethyl-4-chloroacetoacetate, **8**, followed by hydrolysis, through a procedure reported by our group [23,24]. Compound **10** was then reacted with various amino acid methyl esters or 4-aminobenzoic acid methyl ester followed by saponification to produce carboxylic acids **12a–f**. Final condensation with glutamic acid diethyl ester hydrochloride followed by hydrolysis afforded target compounds **1–6**. As an example, compound **6** was characterized to elucidate the structures of our target compounds. The elemental composition of **6** was determined to $C_{20}H_{20}N_6O_7$ from its HRMS (ESI) at m/z 455.1330 [M-H]⁻, which was further verified by the ¹H NMR and ¹³C NMR data (experimental section) suggesting the presence of 20 protons and 20 carbons in **6**. On ¹H NMR spectrum, one singlet at δ_H 6.04 (5-CH) and one broad singlet at δ_H 6.30 (-NH₂), along with the protons at δ_H 11.08 (7-NH) and 10.80 (3-NH), showed pyrrolo[2,3-*d*]pyrimidine core structure. The glutamic acid moiety was indicated as four protons at δ_H 1.92–2.37 (-CH₂-), one proton at δ_H 4.35–4.41 (-CH-), one doublet at δ_H 8.52 (-CONH-) and one broad singlet at δ_H 12.39(-COOH). The double doublet at δ_H 7.75–7.87 (benzene) was attributed to the benzene ring. The singlet present at δ_H 3.66 belonged to methylene group, whereas the singlet at δ_H 10.42 was amide proton. Consequently, **6** was characterized as (S)-2-[4-[2-(2-amino-4-oxo-4,7-dihydro-3H-pyrrolo[2,3-*d*]pyrimidin-6-yl)-acetyl-amino]-benzoylamino]-pentanedioic acid.

3. Biological evaluation and discussion

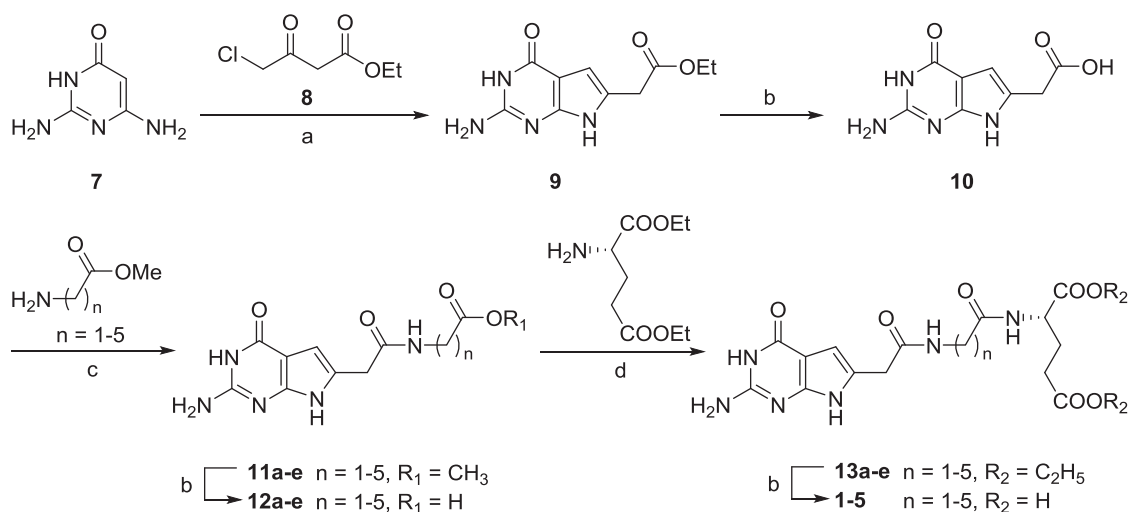
3.1. 6-Substituted pyrrolo [2,3-*d*]pyrimidines as inhibitors of tumor cell proliferation

The newly synthesized compounds **1–6** were initially evaluated for their antiproliferative effects toward a panel of tumor cells including KB (nasopharyngeal), SW620 (colon) and MCF7 (breast) cells through the 3-(4,5-dimethylthiazol-2-yl)-2,5-diphenyltetrazolium bromide (MTT) assay. Cells were

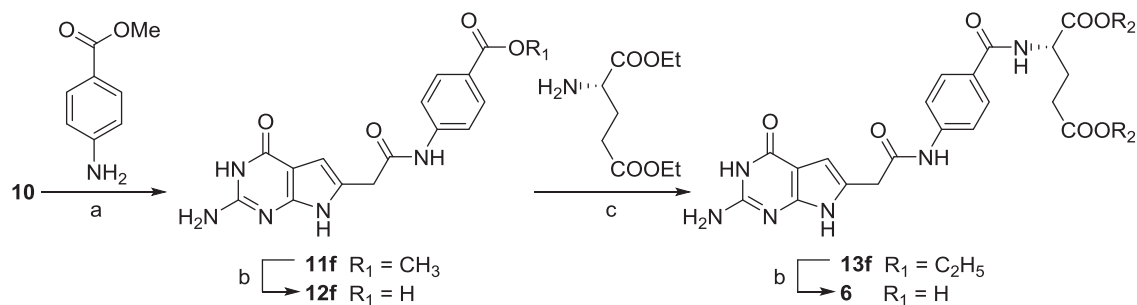
continuously exposed to a wide range of drug concentrations in folate-free RPMI/10% dFBS, supplemented with 2 nM leucovorin [(6*R,S*)-5-formyl tetrahydrofolate (LCV)]. Relative cell numbers were assessed after 72 h. [Table 1](#) was a summary of growth inhibitory effects of compounds **1–6** in comparison with those for the classical antifolates MTX and PMX ([Fig. 1](#)).

As shown in [Table 1](#), compounds **1–6** were all potent inhibitors against KB, SW620 and MCF7 tumor cells. In particular, all compounds demonstrated nanomolar to subnanomolar antiproliferative activities toward KB cells. Compared with the standard MTX (IC₅₀ of 10 nM against KB tumor cells) and PMX (IC₅₀ of 70 nM against KB tumor cells), compound **1** ([Fig. 3](#)), the most potent compound of this series, had an IC₅₀ of 0.078 nM against KB cells in culture, which was about 140-fold and 1000-fold more potent than that of MTX and PMX, respectively. The only benzoyl side chain compound of this series, **6** ([Fig. 3](#)), was also a nanomolar inhibitor against KB cells with an IC₅₀ of 7.5 nM. Compounds **1–6** inhibited proliferation of KB cells in the following order of potency (numbers of bridge carbons are noted in parentheses): **1** (1C) > **5** (5C) > **6** (benzene) > **4** (4C) > **2** (2C) ~ **3** (3C), indicating that the side chain phenyl ring of this series was not necessary for inhibitory activity and could be replaced by a straight chain with even enhanced antitumor activities. A optimal distance of the alkyl amide linker between the core structure of pyrrolo[2,3-*d*]pyrimidine and the L-glutamate moiety is essential. In contrast to the results for KB cells, compounds **1–6** only showed micromolar to submicromolar inhibitory activities toward SW620 and MCF7 cells, which were less potent than of MTX and PMX.

In attempt to confirm that the inhibitory effect of compounds **1–6** leads to cytotoxicity, colony-forming assays were performed towards KB cells and the results were shown in [Fig. 4](#). In these experiments, cells were plated at limiting dilutions, and colonies were counted after 10–14 days. Results were compared with those for KB cells treated with MTX and PMX, and for untreated cells as well. Consistent to the results of inhibition assays ([Table 1](#)), the antiproliferative effects of compounds **1** and **6** were irreversible at the highest concentration, reaching greater than 90% and 80% inhibition of colony formation, respectively ([Fig. 4](#)), thereby establishing these compounds as cytotoxic.



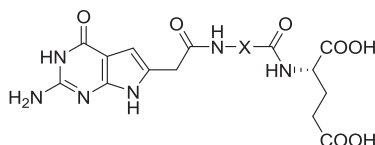
Scheme 1. Reagents and conditions: a) NaOAc, H₂O, reflux, 18 h; b) i) 1 N NaOH, RT, 1.5 h; ii) 3 N HCl; c) EDCI, HOBT, Et₃N, DMF, RT, 5 h; d) NMM, CDMT, DMF, RT, 5 h.



Scheme 2. Reagents and conditions: a) EDCI, HOBT, Et₃N, DMF, RT, 5 h; b) i) 1 N NaOH, RT, 1.5 h; ii) 3 N HCl; c) NMM, CDMT, DMF, RT, 5 h.

Table 1

IC₅₀ values (in μM)^a of 6-substituted pyrrolo[2,3-d]pyrimidines **1–6** and classical antifolates against KB, SW620 and MCF7 cell lines.



antifolate	X	KB	SW620	MCF7
1	-CH ₂ -	7.8×10^{-5} (1×10^{-6})	0.786 (0.029)	0.913 (0.211)
2	-(CH ₂) ₂ -	0.092 (0.006)	1.102 (0.211)	2.375 (0.543)
3	-(CH ₂) ₃ -	0.107 (0.007)	0.948 (0.072)	3.643 (0.821)
4	-(CH ₂) ₄ -	0.043 (0.005)	1.137 (0.142)	3.808 (0.704)
5	-(CH ₂) ₅ -	1.4×10^{-4} (3×10^{-6})	0.563 (0.031)	1.084 (0.137)
6		7.5×10^{-3} (1×10^{-5})	0.977 (0.105)	1.128 (0.150)
MTX	—	0.01 (0.001)	0.022 (0.003)	0.097 (0.006)
PMX	—	0.07 (0.012)	0.09 (0.017)	0.65 (0.028)

^a Calculated from three replicates (plus/minus SEM in parentheses).

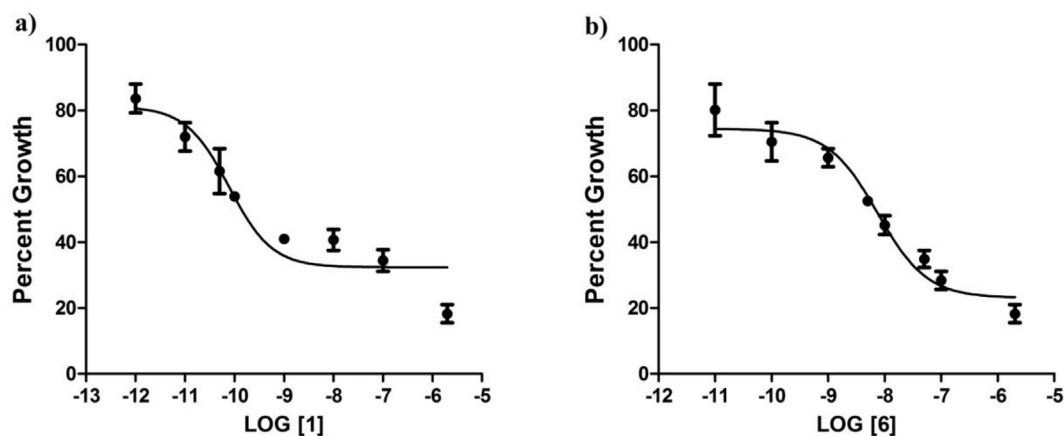


Fig. 3. Growth inhibition of KB cells by compounds **1** and **6** in the presence of physiologic concentrations of reduced folate. a) Growth inhibition of KB cells by compound **1**. b) Growth inhibition of KB cells by compound **6**. Cell proliferation inhibition was measured over a range of concentrations of compounds **1** and **6** in complete folate-free RPMI1640 in the presence of LCV at 2 nM. Cell densities were measured with a MTT assay. Results were normalized to cell density in the absence of drug. Results shown are representative data of experiments performed in triplicate.

3.2. Identification of TS, GARFTase and AICARFTase as the targeted pathway of compound **6**

Nucleoside protection experiments with thymidine (10 μM) and adenosine (60 μM) were conducted to identify the targeted pathway for compound **6**, as that nucleoside salvage pathways

circumvent the biosynthetic requirements for reduced folates. If TS and/or purine biosynthesis are targeted, the inhibitory effects of the new series of compounds against KB cells would be abolished by excessive thymidine or adenosine. In addition, KB cells were also treated with 5-aminoimidazole-4-carboxamide (AICA, 320 μM) in the presence of compound **6** to confirm the likely targets in purine

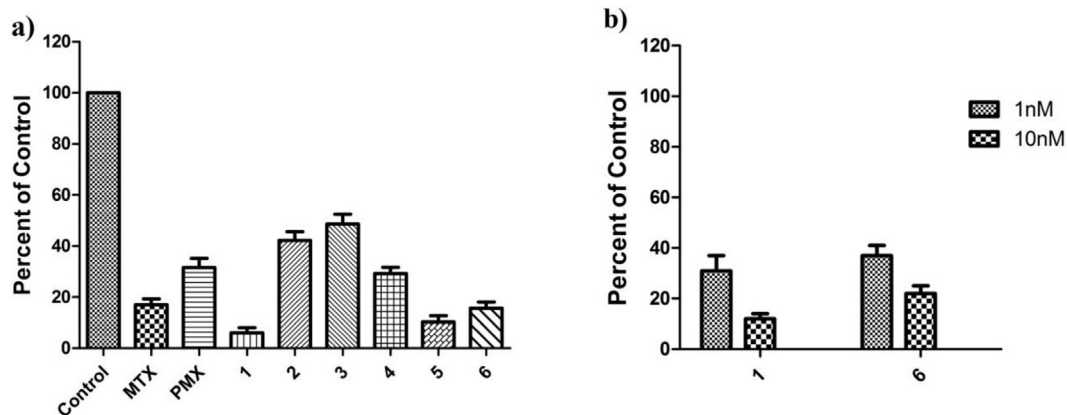


Fig. 4. Colony-forming inhibition assay. a) KB cells were inoculated into 60 mm dishes with a density of 300 cells per dish, in the presence of MTX (10 nM), PMX (100 nM) or compounds **1–6** (100 nM). b) The percentage of colony-forming in the presence of compounds **1** and **6** (1 nM and 10 nM). Colonies were enumerated after 10–14 days after staining with methylene blue. Data were calculated as percent of controls treated identically but without drugs. Results are presented as mean values from three experiments (plus/minus SEM).

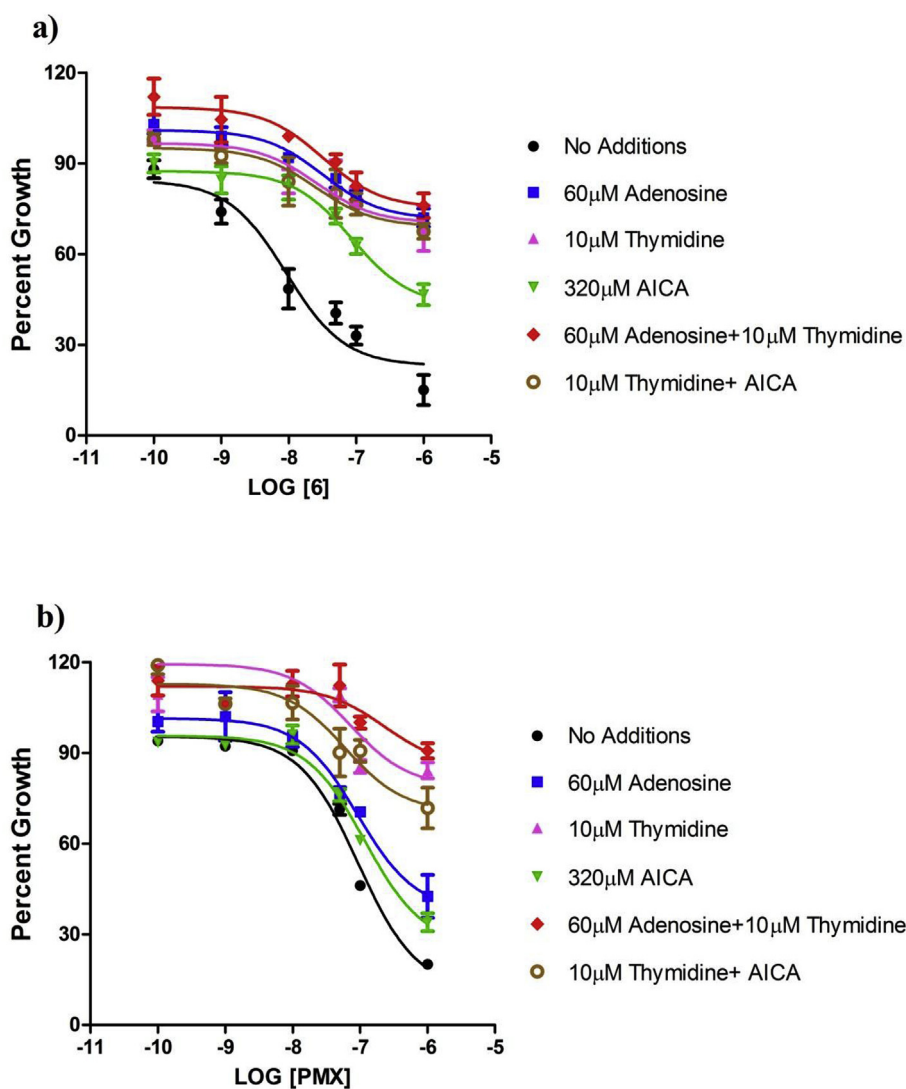


Fig. 5. Cell proliferation assays with protection by nucleosides including thymidine and adenosine and by 5-aminoimidazole-4-carboxamide (AICA) to identify intracellular targets of PMX and compound **6**. To identify the targeted pathways and the folate-dependent intracellular enzymes in KB cells treated with compound **6** (1 nM–10 μM), cell proliferation assays were performed in the presence of 10 μM thymidine, 60 μM adenosine, or 320 μM AICA. a) The results for **6**, normalized to those for untreated cells (no drug). b) The results for PMX. Details are provided in the Experimental section. The results shown are representative of triplicate experiments.

nucleotide biosynthesis (GARFTase versus AICARFTase). In cells, AICA is metabolized to AICAR, the substrate for AICARFTase, therefore it would bypass the step catalyzed by GARFTase.

Fig. 5 shows the nucleoside/AICA protection results for compound **6** compared to those for PMX. As reported in literature, PMX is a multitargeted antifolate against TS, DHFR, GARFTase and AICARFTase. The experiment data clearly showed that the growth inhibitory effect of the PMX with KB cells was partially protected by excess thymidine and adenosine, but was completely reversed in the presence of combined thymidine and adenosine. Similar results were obtained for compound **6** in that single addition of excess thymidine or adenosine was partially protective in different extent, while combined thymidine and adenosine completely protected KB cells from the growth inhibitory effects of **6**, indicating that both thymidylate and de novo purine nucleotide synthesis was being targeted. For PMX and compound **6**, AICA alone or combined with thymidine was only partially protective, suggesting that inhibition of purine nucleotide biosynthesis by these two compounds is likely a composite effect of dual inhibitions involving both GARFTase and AICARFTase. Therefore, the results strongly imply that compound **6** is a multitargeted antifolate targeting TS, GARFTase and AICARFTase. Nucleoside protection experiments of the non-benzoyl straight chain compounds **1** and **5** were also performed to identify their molecular targets. Similar to the results of **6**, the antiproliferative activity of compounds **1** and **5** was attributable to multitargeted inhibition of folate-dependent enzymes TS, GARFTase and AICARFTase (Fig. S1 and Fig. S2, Supplementary Material).

3.3. Effect of compounds **1** and **6** on cell cycle progression and apoptosis in KB cells

Studies of cell cycle with apoptosis are of key importance in understanding intracellular mechanism of action of antitumor chemotherapies. In KB cells, etoposide, a topoisomerase II inhibitor [26], induced S-phase inhibition and G1-phase accumulation [23], whereas, PMX, a multitargeted antifolate, resulted in cell cycle arrest at G1-phase with G2-phase suppression [23]. To explore the impact of folate-dependent enzyme inhibition of the synthesized compounds on cell-cycle progression, KB cells were treated with compound **1** (1 μ M) and compound **6** (1 μ M), along with etoposide (5 μ M), PMX (10 μ M) and a vehicle control for 96 h. Then, cells were washed, fixed, stained with propidium iodide (PI), and analyzed for cell cycle distribution by flow cytometry. Similar to the result of PMX, treatment of compound **1** or **6** caused G2-phase inhibition such that the G2-fraction decreased from 9.59% in the absence of drugs to 2.43% with compound **1**, even disappeared with PMX or compound **6** (Fig. 6). For the S-population, treatment of compound **1** or **6** significantly increased cell distribution from 35.66% to 44.96% and 68.62%, respectively (Fig. 6). The G1-fraction decreased upon treatment with compound **1** or **6** from 54.75% and 31.38%, respectively, yet slightly increased to 61.95% with PMX (Fig. 6). The results suggested that compound **1** and **6** induced cell cycle arrest at S-phase with G2-phase suppression.

KB cells were stained with annexin V-FITC/PI and analyzed by flow cytometry to monitor the induction of apoptosis by our newly synthesized compounds. It has been reported that PMX induces

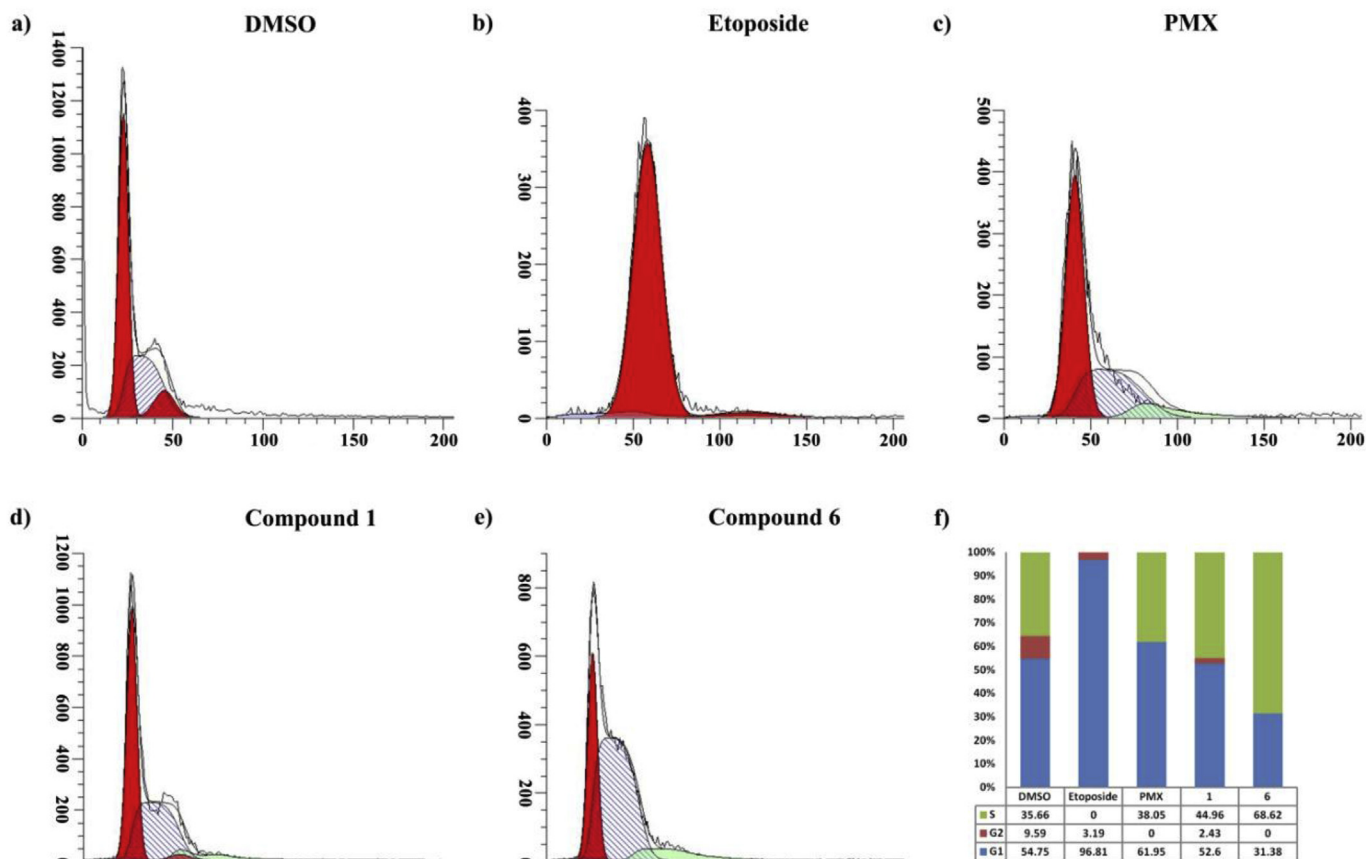


Fig. 6. Cell cycle assay. KB were treated with etoposide (5 μ M), PMX (10 μ M), compound **1** (1 μ M), compound **6** (1 μ M) or left untreated (DMSO) for 96 h, washed, fixed, and stained with PI. Cell cycle distributions were analyzed by flow cytometry. Cell cycle distributions: a) DMSO, b) etoposide, c) PMX, d) compound **1**, e) compound **6**, f) The percentages of cells in each phase of the cell cycle (G1, S, and G2).

both intrinsic and extrinsic apoptosis through a p53-mediated and caspase-dependent and -independent signaling pathways [27]. As shown in Fig. 7, KB cells treated with PMX showed significant increases in both early- and late-apoptotic fractions compared those for the untreated control (i.e., the fractions of cells in early apoptosis were 67% and 16.9% for PMX-treated and control cells, respectively, whereas the fractions in late apoptosis at 48 h were 21.8% and 5.5%, respectively). The results also demonstrated that both compound **1** and **6** could induce distinct early apoptosis (35.4% and 36.2% for compound **1** and **6**, respectively) but no late apoptosis (Fig. 7), which is different from the result of PMX.

3.4. Molecular modeling

To provide a molecular explanation for the cellular metabolic data that compound **6** inhibits TS, GARFTase and AICARFTase in KB cells, MOE 2009.10 was used to perform molecular modeling studies, and the docked poses were visualized using CCP4MG [28].

Fig. 8 shows the docked pose of compound **6** (red) in the human GARFTase active site (PDB ID 4ZZ3). The pyrrolo[2,3-*d*]pyrimidine scaffolds of **6** and PMX occupy the same location. Analogous to

PMX, the 2-NH₂ moiety forms a hydrogen bond with the side chain of α -carboxylic group of Glu948, whereas 3-NH interacts with the backbone of Ala947. The 4-oxo moiety forms two hydrogen bonds with both Asp951 and H₂O1216. Additional hydrogen bond is formed between 7-NH of the pyrrolo[2,3-*d*]pyrimidine and the backbone of Arg897. The side chain amide carbonyl oxygen of **6** has a hydrogen bond interaction with Asn913. The glutamate side chain of **6** is oriented similarly to that of PMX, and forms two hydrogen bonds with the backbone of Met896 and the side chain of Arg897, respectively.

The docked pose of compound **6** (red) in the human AICARFTase active site (PDB ID 1P4R) was shown in Fig. 9. Similar to the quinazolinone ring of the native crystal structure ligand (BW1540, Fig. 1), the pyrrolo[2,3-*d*]pyrimidine scaffold of **6** resides in a pocket formed by Phe544, Asn489, Met312, Asp546, Ile452 and Ser450. This orientation of the scaffold permits the 2-NH₂ moiety to form hydrogen bonds to the side chains of Asp546, whereas the 4-oxo moiety forms a hydrogen bond with the side chain of Asn547. The side chain benzoic carbonyl oxygen of **6** interacts with H₂O1815 and H₂O1947 to form hydrogen bonds. Similar to BW1540, the glutamate moiety of **6** is oriented in a manner that aids the α -carboxylic

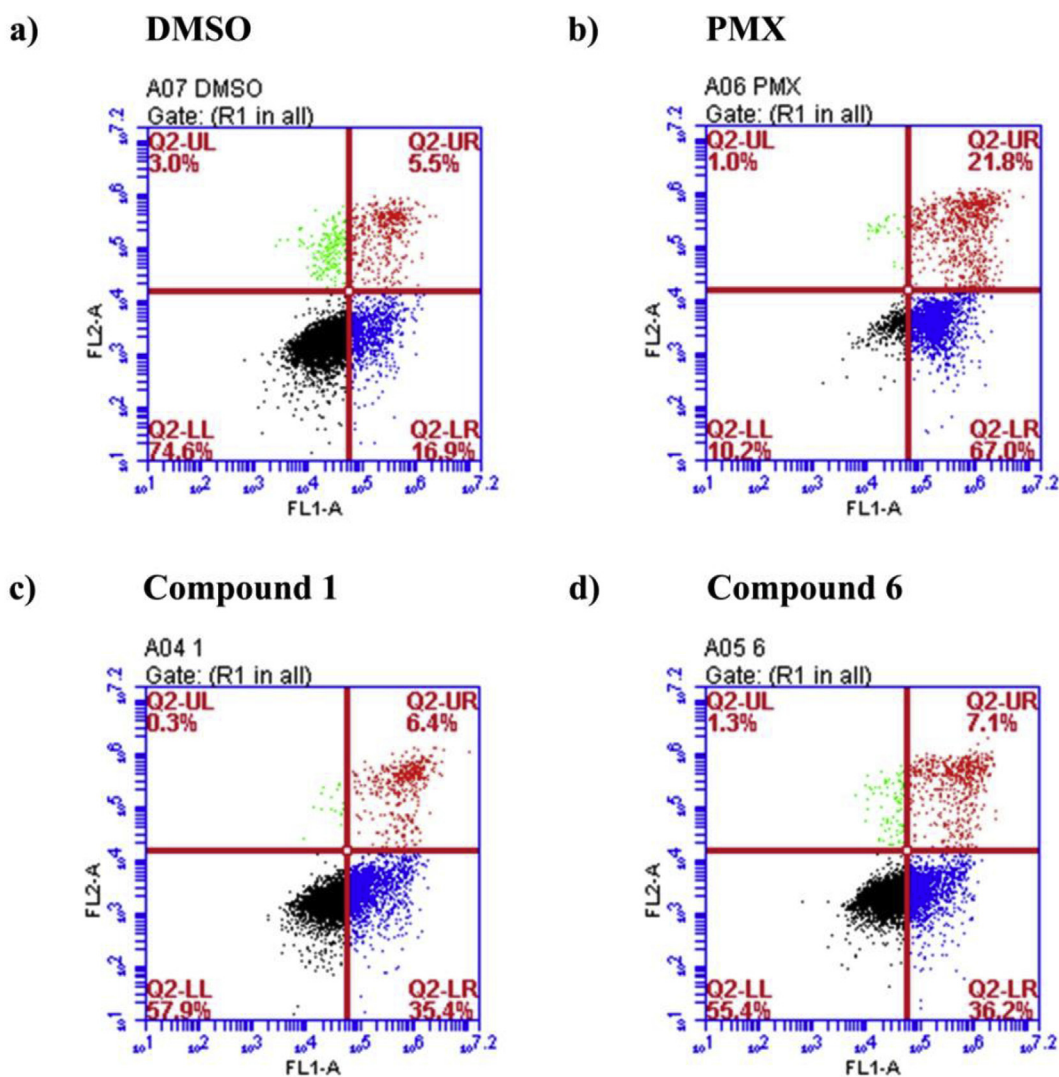


Fig. 7. Apoptosis in KB cells treated with PMX, compound **1** or **6** for 48 h. Apoptosis was analyzed using annexin V-FITC/PI staining and flow cytometry for early apoptosis (Q2-LR), late apoptosis (Q2-UR) and necrosis (Q2-UL); viable cells are shown in Q2-LL. Results are compared to those for controls treated with DMSO. The percentages of cells in each quadrant are summarized. a) DMSO, b) PMX, c) compound **1**, d) compound **6**.

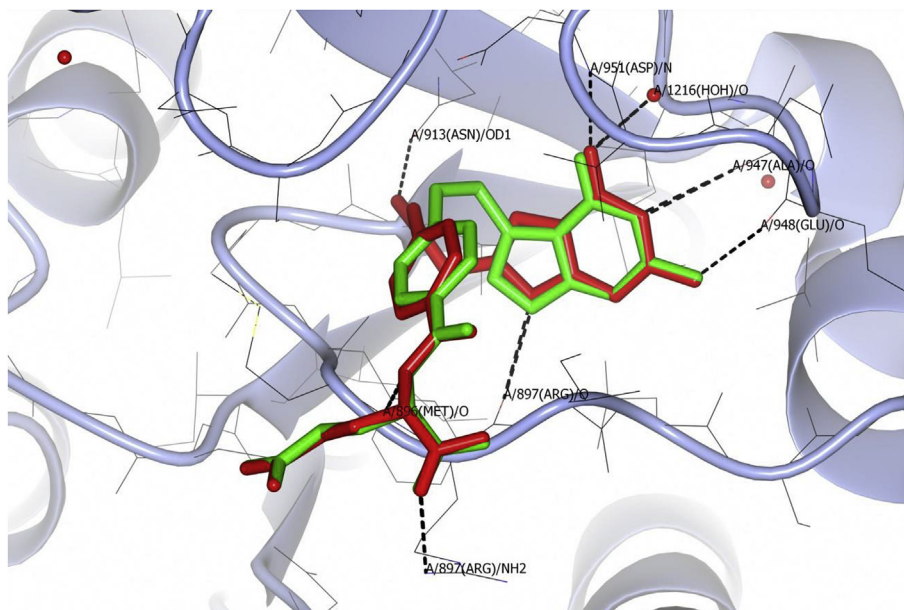


Fig. 8. Molecular modeling of **6** with GARFTase. Docked pose of **6** (red) with PMX (green) in human GARFTase (PDB ID 4ZZ3). (For interpretation of the references to colour in this figure legend, the reader is referred to the web version of this article.)

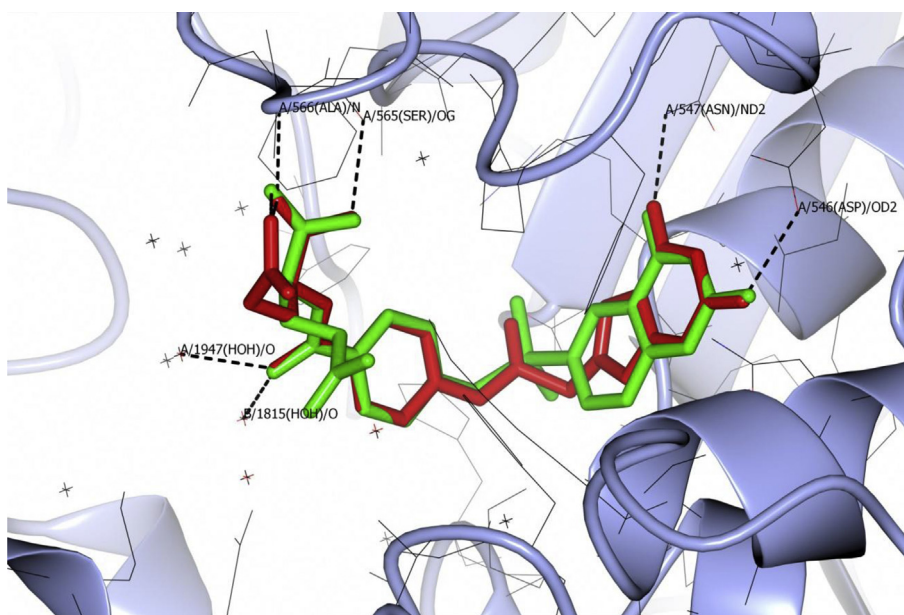


Fig. 9. Molecular modeling of **6** with AICARFTase. Docked pose of **6** (red) with BW1540 (green) in human AICARFTase (PDB ID 1P4R). (For interpretation of the references to colour in this figure legend, the reader is referred to the web version of this article.)

group form two hydrogen bonds with the backbone of Ala566 and the side chain of Ser565, respectively.

Fig. 10 shows the overlay of the docked poses of **6** (red) with the crystal structure of PMX (green) in human TS (PDB ID 1JU6). The results show that the pyrrolo[2,3-*d*]pyrimidine scaffold of **6** occupies the same location as that of PMX and are buried deep in the active site. For the pyrrolo[2,3-*d*]pyrimidine core of **6**, several important hydrogen bond interactions are involved. The N1 nitrogen forms a hydrogen bond with H₂O435, whereas the 2-NH₂ interacts with the backbone of Ala312. The N7 nitrogen of **6** forms a hydrogen bond with the side chain of Asn112. The glutamate side chains of **6** and PMX are oriented similarly.

Consistent with the results of our *in vitro* metabolic assays (Fig. 5), the docking results clearly demonstrate that compound **6** could bind and inhibit both *de novo* purine biosynthetic enzymes (i.e., GARFTase and AICARFTase) and TS.

4. Conclusions

In this paper, we reported the design, synthesis, biological evaluation and molecular modeling of a novel series of 6-substituted benzoyl and non-benzoyl straight chain pyrrolo[2,3-*d*]pyrimidines as potential antitumor agents targeting both thymidylate and purine nucleotide biosynthesis. The newly synthesized

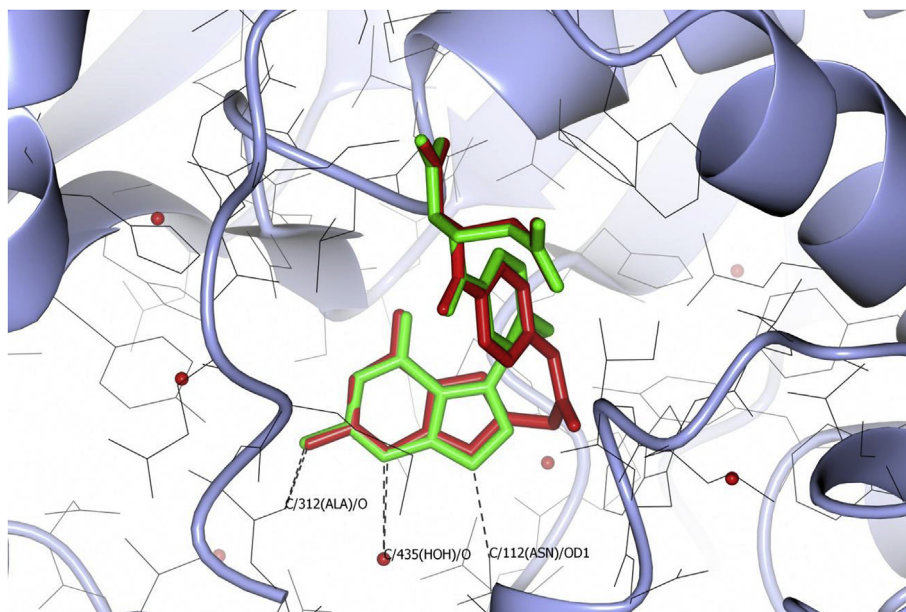


Fig. 10. Molecular modeling of **6** with TS. Docked pose of **6** (red) with PMX (green) in human TS (PDB ID 1JU6). (For interpretation of the references to colour in this figure legend, the reader is referred to the web version of this article.)

compounds showed antiproliferative potencies against a panel of tumor cell lines including KB, SW620 and MCF7, whereas most compounds of this series exhibited nanomolar to subnanomolar inhibitory activities toward KB tumor cells. Particularly, compound **1**, the most potent compounds of this series, has an IC_{50} of 0.078 nM against KB cells in culture, which is about 140-fold and 1000-fold more potent than that of the positive control MTX (IC_{50} of 10 nM against KB tumor cells) and PMX (IC_{50} of 70 nM against KB tumor cells), respectively. The results also established that the side chain phenyl ring of a classical antifolate was not necessary and could be replaced by a straight chain with even enhanced antitumor activities. An optimal distance of the alkyl amide linker between the core structure of pyrrolo[2,3-*d*]pyrimidine and the *L*-glutamate moiety is essential. Consistent with the results of nucleoside protection assays, molecular modeling studies demonstrated that inhibition of cell proliferation was attributable to multitargeted inhibition of folate-dependent enzymes TS, GARFTase and AICARFTase. Growth inhibition induced distinct early apoptosis and cell cycle arrest at S-phase, leading to cell death. The subnanomolar antitumor activities and structural simplicity of our non-benzoyl straight chain compounds provide an excellent starting point for further study, including rational design of additional potent multitargeted antifolates to optimize inhibition of folate metabolizing enzymes toward discovering new generation of antitumor agents.

5. Experimental section

5.1. Chemistry

All evaporations were carried out *in vacuo* with a rotary evaporator. Analytical samples were dried in a Buchi B-585 vacuum (0.2 mmHg) drying oven over P_2O_5 . Melting points were determined on a Digital Melting Point apparatus (Buchi M-560) and were uncorrected. 1H NMR spectra were recorded on a Bruker Avance III 400 MHz NMR spectrometer. The chemical shift values were expressed in ppm (parts per million) relative to tetramethylsilane as internal standard; s = singlet, d = doublet, t = triplet, q = quartet, m = multiplet, br = broad singlet. The relative integrals

of peak areas agreed with those expected for the assigned structures. ^{13}C NMR spectra were recorded on a Bruker Avance II 100 MHz NMR spectrometer. Low resolution mass spectra (LRMS) were determined on an ABI 3200 Qtrap mass spectrometer, and high resolution mass spectra (HRMS) were determined on an AB SCIEX Triple TOF 5600⁺ mass spectrometer. Thin-layer chromatography (TLC) was carried out on Silica Gel GF254 plates, and the spots were visualized under 254 and 365 nm illumination. Column chromatography was taken on 230–400 mesh silica gel. Analytical HPLC was performed on an Agilent 1200 equipped with a Diode Array Detector (DAD). All solvents and chemicals were purchased from Aldrich Chemical Co. and Fisher Scientific and were used as received. Purities of all assayed compounds were determined by analytical HPLC and were found to be $\geq 95\%$ pure unless otherwise specified.

5.1.1. General procedure for the synthesis of target compounds **1–6**

To a solution of previously synthesized intermediates **12a–12f** (1.0 mmol) in anhydrous DMF (10 mL) was added *N*-methylmorpholine (182 mg, 1.8 mmol) and 2-chloro-4,6-dimethoxy-1,3,5-triazine (317 mg, 1.8 mmol). The resulting mixture was stirred at room temperature for 2 h. To this mixture was added *N*-methylmorpholine (182 mg, 1.8 mmol) and *L*-glutamate diethyl ester hydrochloride (360 mg, 1.5 mmol). The reaction mixture was stirred for an additional 4 h at room temperature. Silica gel (600 mg) was then added, and the solvent was evaporated under reduced pressure. The resulting plug was loaded on to a silica gel column (1.5 × 15 cm) with 5% $CHCl_3$ in MeOH as the eluent. Fractions that showed the desired spot (TLC) were pooled, and the solvent evaporated to dryness to afford a residue. To this residue was added MeOH (10 mL) and 1 N NaOH (10 mL), then the mixture was stirred under N_2 at room temperature for 16 h. TLC showed the disappearance of the starting material ($R_f = 0.15$) and one major spot at the origin ($CHCl_3/MeOH$ 10:1). The reaction mixture was then evaporated to dryness under reduced pressure. The residue was dissolved in water (10 mL), the resulting solution was cooled in an ice bath, and the pH was adjusted to 3–4 with dropwise addition of 1 N HCl. The resulting suspension was frozen in a dry ice-acetone

bath, thawed to 4–5 °C in the refrigerator, and filtered. The residue was washed with a small amount of cold water and dried in vacuum using P₂O₅ to afford **1–6** as white to yellow powder.

5.1.1.1. (*S*)-2-[2-[2-(2-Amino-4-oxo-4,7-dihydro-3H-pyrrolo [2,3-*d*] pyrimidin-6-yl)-acetylaminol]-acetylaminol]-pentanedioic acid (**1**). Compound **1** was prepared using the general method described for the preparation of **1–6** from **12a** (265 mg, 1.0 mmol) to give **1** as a off-white powder (184 mg, 46.7%); mp: 215 °C; ¹H NMR (400 MHz, DMSO-*d*₆): δ = 1.76–1.96 (m, 2H, CH₂), 2.24–2.27 (m, 2H, CH₂), 3.60–3.74 (m, 4H, CH₂), 4.16–4.21 (m, 1H, CH), 6.00 (s, 1H, 5-H), 6.19 (s, 2H, 2-NH₂), 8.08–8.12 (m, 2H, CONH), 10.38 (s, 1H, 3-H), 10.83 (s, 1H, 7-H), 11.93 (br, 2H); ¹³C NMR (100 MHz, DMSO-*d*₆): δ = 26.84, 30.30, 34.88, 42.03, 51.64, 99.84, 100.18, 124.64, 149.91, 151.19, 152.30, 158.58, 168.67, 169.40, 173.97; ESI-MS (*m/z*): 393.1 [M - H]⁻; HRMS (ESI): calcd for C₁₅H₁₇N₆O₇ [M - H]⁻, 393.1164; found, 393.1181.

5.1.1.2. (*S*)-2-[3-[2-(2-Amino-4-oxo-4,7-dihydro-3H-pyrrolo [2,3-*d*] pyrimidin-6-yl)-acetylaminol]-propionylaminol]-pentanedioic acid (**2**). Compound **2** was prepared using the general method described for the preparation of **1–6** from **12b** (280 mg, 1.0 mmol) to give **2** as a off-white powder (175 mg, 43%); mp: 280 °C; ¹H NMR (400 MHz, DMSO-*d*₆): δ = 1.74–1.92 (m, 2H, CH₂), 2.24–2.31 (m, 4H, CH₂), 3.19–3.28 (m, 2H, CH₂), 3.33 (s, 2H, CH₂), 4.15–4.21 (m, 1H, CH), 5.95 (s, 1H, 5-H), 6.08 (s, 2H, 2-NH₂), 7.93–7.96 (t, 1H, *J* = 5.2 Hz, CONH), 8.03–8.04 (d, 1H, *J* = 7.6 Hz, CONH), 10.25 (s, 1H, 3-H), 10.86 (s, 1H, 7-H), 12.93 (br, 2H); ¹³C NMR (100 MHz, DMSO-*d*₆): δ = 28.10, 32.67, 39.64, 40.79, 41.54, 56.01, 99.73, 123.41, 124.71, 147.98, 148.58, 151.11, 152.02, 158.43, 167.48, 173.98; ESI-MS (*m/z*): 407.1 [M - H]⁻; HRMS (ESI): calcd for C₁₆H₁₉N₆O₇ [M - H]⁻, 407.1321; found, 407.1333.

5.1.1.3. (*S*)-2-[4-[2-(2-Amino-4-oxo-4,7-dihydro-3H-pyrrolo [2,3-*d*] pyrimidin-6-yl)-acetylaminol]-butyrylamino]-pentanedioic acid (**3**). Compound **3** was prepared using the general method described for the preparation of **1–6** from **12c** (294 mg, 1.0 mmol) to give **3** as a yellow powder (187 mg, 44.4%); mp: 217 °C; ¹H NMR (400 MHz, DMSO-*d*₆): δ = 1.59–1.66 (m, 2H, CH₂), 1.72–1.94 (m, 2H, CH₂), 2.11–2.15 (t, 2H, *J* = 7.6 Hz, CH₂), 2.25–2.28 (t, 2H, *J* = 7.6 Hz, CH₂), 3.00–3.09 (m, 2H, CH₂), 3.33 (s, 2H, CH₂), 4.15–4.20 (m, 1H, CH), 5.95 (s, 1H, 5-H), 6.08 (s, 2H, 2-NH₂), 7.91–7.93 (t, 1H, *J* = 5.2 Hz, CONH), 8.02–8.04 (d, 1H, *J* = 7.6 Hz, CONH), 10.24 (s, 1H, 3-H), 10.85 (s, 1H, 7-H), 12.57 (br, 2H); ¹³C NMR (100 MHz, DMSO-*d*₆): δ = 18.53, 25.38, 26.71, 32.70, 34.99, 38.37, 51.31, 55.99, 99.84, 125.02, 133.21, 151.11, 152.03, 158.46, 168.88, 173.51, 173.86; ESI-MS (*m/z*): 421.2 [M - H]⁻; HRMS (ESI): calcd for C₁₇H₂₁N₆O₇ [M - H]⁻, 421.1477; found, 421.1471.

5.1.1.4. (*S*)-2-[5-[2-(2-Amino-4-oxo-4,7-dihydro-3H-pyrrolo [2,3-*d*] pyrimidin-6-yl)-acetylaminol]-pentanoylamino]-pentanedioic acid (**4**). Compound **4** was prepared using the general method described for the preparation of **1–6** from **12d** (307 mg, 1.0 mmol) to give **4** as a yellow powder (252 mg, 57.7%); mp: 221 °C; ¹H NMR (400 MHz, DMSO-*d*₆): δ = 1.37–1.42 (m, 2H, CH₂), 1.45–1.53 (m, 2H, CH₂), 1.70–1.99 (m, 2H, CH₂), 2.10–2.14 (t, 2H, *J* = 7.2 Hz, CH₂), 2.25–2.29 (t, 2H, *J* = 8.0 Hz, CH₂), 3.01–3.06 (m, 2H, CH₂), 3.33 (s, 2H, CH₂), 4.18–4.22 (m, 1H, CH), 5.95 (s, 1H, 5-H), 6.05 (s, 2H, 2-NH₂), 7.82–7.84 (t, 1H, *J* = 5.2 Hz, CONH), 8.07–8.09 (d, 1H, *J* = 8.0 Hz, CONH), 10.21 (s, 1H, 3-H), 10.82 (s, 1H, 7-H), 12.37 (br, 2H); ¹³C NMR (100 MHz, DMSO-*d*₆): δ = 22.68, 26.29, 28.62, 30.07, 34.63, 34.96, 38.47, 51.01, 99.75, 99.84, 125.13, 151.09, 151.98, 158.49, 168.76, 172.21, 173.42, 173.67; ESI-MS (*m/z*): 435.2 [M - H]⁻; HRMS (ESI): calcd for C₁₈H₂₃N₆O₇ [M - H]⁻, 435.1634; found, 435.1643.

5.1.1.5. (*S*)-2-[6-[2-(2-Amino-4-oxo-4,7-dihydro-3H-pyrrolo [2,3-*d*] pyrimidin-6-yl)-acetylaminol]-hexanoylamino]-pentanedioic acid (**5**). Compound **5** was prepared using the general method described for the preparation of **1–6** from **12e** (321 mg, 1.0 mmol) to give **5** as a off-white powder (375 mg, 83.3%); mp: 148 °C; ¹H NMR (400 MHz, DMSO-*d*₆): δ = 1.18–1.26 (m, 2H, CH₂), 1.36–1.41 (m, 2H, CH₂), 1.45–1.50 (m, 2H, CH₂), 1.71–1.99 (m, 2H, CH₂), 2.09–2.13 (t, 2H, *J* = 7.2 Hz, CH₂), 2.26–2.29 (t, 2H, *J* = 7.2 Hz, CH₂), 3.00–3.04 (m, 2H, CH₂), 3.33 (s, 2H, CH₂), 4.16–4.23 (m, 1H, CH), 5.95 (s, 1H, 5-H), 6.17 (s, 2H, 2-NH₂), 7.88–7.90 (t, 1H, *J* = 4.8 Hz, CONH), 8.07–8.09 (d, 1H, *J* = 7.6 Hz, CONH), 10.31 (s, 1H, 3-H), 10.86 (s, 1H, 7-H), 12.35 (br, 2H); ¹³C NMR (100 MHz, DMSO-*d*₆): δ = 24.91, 25.97, 26.30, 28.77, 30.13, 34.96, 35.04, 38.62, 51.05, 99.75, 99.83, 125.10, 151.08, 152.12, 158.46, 168.79, 172.31, 173.41, 173.66; ESI-MS (*m/z*): 449.2 [M - H]⁻; HRMS (ESI): calcd for C₁₉H₂₅N₆O₇ [M - H]⁻, 449.1790; found, 449.1783.

5.1.1.6. (*S*)-2-[4-[2-(2-Amino-4-oxo-4,7-dihydro-3H-pyrrolo [2,3-*d*] pyrimidin-6-yl)-acetylaminol]-benzoylamino]-pentanedioic acid (**6**). Compound **6** was prepared using the general method described for the preparation of **1–6** from **12f** (327 mg, 1.0 mmol) to give **6** as a off-white powder (264 mg, 57.8%); mp: 204 °C; ¹H NMR (400 MHz, DMSO-*d*₆): δ = 1.92–2.13 (m, 2H, CH₂), 2.34–2.37 (t, 2H, *J* = 7.2 Hz, CH₂), 3.66 (s, 2H, CH₂), 4.35–4.41 (m, 1H, CH), 6.04 (s, 1H, 5-H), 6.30 (s, 2H, 2-NH₂), 7.75–7.87 (dd, 4H, benzene), 8.52–8.53 (d, 1H, *J* = 7.2 Hz, CONH), 10.42 (s, 1H, CONH), 10.80 (s, 1H, 3-H), 11.08 (s, 1H, 7-H), 12.39 (br, 2H); ¹³C NMR (100 MHz, DMSO-*d*₆): δ = 25.90, 30.46, 36.13, 51.92, 99.79, 100.30, 118.09, 124.23, 128.24, 142.18, 151.14, 152.35, 158.41, 165.99, 168.43, 173.42, 173.82; ESI-MS (*m/z*): 455.1 [M - H]⁻; HRMS (ESI): calcd for C₂₀H₁₉N₆O₇ [M - H]⁻, 455.1321; found, 455.1330.

5.2. Biological evaluation

5.2.1. Cell culture

KB cells were obtained from American Type Culture Collection (ATCC). SW620 and MCF7 cells were obtained from Type Culture Collection of the Chinese Academy of Sciences (Shanghai, China). KB, SW620 and MCF7 cells were routinely cultured in folate-free RPMI1640 medium, supplemented with 10% fetal bovine serum, penicillin-streptomycin solution, and 2 mM L-glutamine at 37 °C with 5% CO₂.

5.2.2. Growth inhibition assays

To evaluate antiproliferative properties of the synthesized compounds, the 3-(4,5-dimethylthiazol-2-yl)-2,5-diphenyltetrazolium bromide (MTT) assay was used. The cell lines were assessed by trypsinizing each cell line and seeding 4 × 10³ cells per well into 96-well plates. Cells were grown for 24 h and then treated with compounds at concentrations ranging from 1 nM to 10 μM and incubated for 72 h in 200 μL media. MTT reagent (20 μL) in serum-free medium (5 mg/mL) was added to each well and incubated further for 4 h. Media was removed, and the resulting formazan crystals were re-solubilized in 200 μL of DMSO. A₄₉₀ was measured using a Thermomax Molecular Device plate reader. The experiments were performed in quadruplicate and repeated at least three times for each compound per cell line. Cells treated with 0.1% DMSO were used as a control, while MTX and PMX were used as positive controls.

5.2.3. Nucleosides protection assays

The inhibitory effects of the antifolate inhibitors on de novo thymidylate biosynthesis (i.e., TS) and de novo purine biosynthesis (GARFTase and AICARFTase) were tested by coincubations with thymidine (10 μM) and adenosine (60 μM), respectively. For de

novo purine biosynthesis, additional protection experiments used AICA (320 μ M) as a means of distinguishing inhibitory effects at GARFTase from those at AICARFTase.

5.2.4. Assessment of cell cycle distribution and apoptosis

KB cells were treated with 1 μ M compound **1**, 1 μ M compound **6**, 5 μ M etoposide and 10 μ M PMX for 96 h in complete folate-free RPMI 1640 medium/10% dFBS and 2 nM LCV. Cells were trypsinized, pelleted, and washed once with ice-cold DPBS. Cells (1×10^6) were fixed in ethanol (-20 °C, overnight), then stained by resuspension in 0.5 ml of DPBS containing 50 μ g/ml PI and 100 μ g/ml RNase type I-A (Sigma Aldrich). The cells were analyzed by flow cytometry for determining the percentage of cells in each phase of the cell cycle. In each experiment, 1×10^4 cells were assessed for cell cycle distribution. Apoptosis was measured using the annexin V-FITC/PI kit, as specified by the manufacturer (BD Biosciences), with a minimum of 20,000 events (cells) analyzed for early apoptosis (Q1-LR), late apoptosis (Q1-UR) and necrosis (Q1-UL); viable cells are shown in Q1-LL. All data were analyzed with ModFit LT (v4.0) software (VeritySoftwareHouse).

5.3. Molecular modeling

The X-ray crystal structures of human GARFTase at 2.5 Å resolution (PDB ID 4ZZ3), human AICARFTase at 2.55 Å resolution (PDB ID 1P4R) and human TS at 2.89 Å resolution (PDB ID 1JU6) were obtained from the Protein Data Bank. Docking studies were performed using MOE 2009.10. The reference ligands (PMX and BW1540) were redocked into their binding sites of human TS, GARFTase and AICARFTase respectively to validate the docking studies. The results were shown in Fig. S3, Fig. S4, and Fig. S5 in Supplementary Material. The protonation state of the proteins and the ligands were calculated using the default settings. Water molecules in the active site were permitted to rotate freely. The active site was defined by a sphere of 6.5 Å from the native ligand in the crystal structure. Molecules used for the docking experiments were prepared using MOE and energy-minimized using the MMF94 \times force field to a constant of 0.05 kcal/mol. Triangle matching was used as the placement method, and the docked poses were scored using default settings. The docked poses were visualized using CCP4MG.

Acknowledgments

This work was supported by the National Natural Science Foundation of China (21507022, 81202401, 21502041, 81473292); Natural Science Foundation of Hebei Province, China (H2017206291, H2014206310), Educational Commission of Hebei Province, China (ZD2015112) and Department of Human Resources and Social Security of Hebei Province, China (C2013003026, C201400329).

Appendix A. Supplementary data

Supplementary data related to this article can be found at <http://dx.doi.org/10.1016/j.ejmech.2017.08.032>.

References

- [1] N. Gonen, Y.G. Assaraf, Antifolates in cancer therapy: structure, activity and mechanisms of drug resistance, *Drug Resist. Updat.* 15 (2012) 183–210.
- [2] M. Visentin, R. Zhao, I.D. Goldman, The antifolates, *Hematol. Oncol. Clin. North Am.* 26 (2012) 629–648 ix.
- [3] N. Hagner, M. Joerger, Cancer chemotherapy: targeting folic acid synthesis, *Cancer Manag. Res.* 2 (2010) 293–301.
- [4] N. Tzioumaki, S. Manta, E. Tsoukala, V.V. Johan, S. Liekens, D. Komiotis, J. Balzarini, Synthesis and biological evaluation of unsaturated keto and exo-methylene d-arabinopyranonucleoside analogs: novel 5-fluorouracil analogs that target thymidylate synthase, *Eur. J. Med. Chem.* 46 (2011) 993–1005.
- [5] Q.-R. Du, D.-D. Li, Y.-Z. Pi, J.-R. Li, J. Sun, F. Fang, W.-Q. Zhong, H.-B. Gong, H.-L. Zhu, Novel 1,3,4-oxadiazole thioether derivatives targeting thymidylate synthase as dual anticancer/antimicrobial agents, *Biorg. Med. Chem.* 21 (2013) 2286–2297.
- [6] H.I. El-Subbagh, G.S. Hassan, S.M. El-Messery, S.T. Al-Rashood, F.A.M. Al-Omary, Y.S. Abulfadl, M.I. Shabayek, Nonclassical antifolates, part 5. Benzodiazepine analogs as a new class of DHFR inhibitors: synthesis, antitumor testing and molecular modeling study, *Eur. J. Med. Chem.* 74 (2014) 234–245.
- [7] X. Zhou, K. Lin, X. Ma, W.-K. Chui, W. Zhou, Design, synthesis, docking studies and biological evaluation of novel dihydro-1,3,5-triazines as human DHFR inhibitors, *Eur. J. Med. Chem.* 125 (2017) 1279–1288.
- [8] A. Bhosle, N. Chandra, Structural analysis of dihydrofolate reductases enables rationalization of antifolate binding affinities and suggests repurposing possibilities, *FEBS J.* 283 (2016) 1139–1167.
- [9] J. Chon, P.J. Stover, M.S. Field, Targeting nuclear thymidylate biosynthesis, *Mol. Asp. Med.* DOI: 10.1016/j.mam.2016.11.005.
- [10] G.S. Wood, J. Wu, Methotrexate and pralatrexate, *Dermatol. Clin.* 33 (2015) 747–755.
- [11] S.M. Malik, K. Liu, X. Qiang, R. Sridhara, S. Tang, W.D. McGuinn Jr., S.L. Verbois, A. Marathe, G.M. Williams, J. Bullock, C. Tornoe, S.C. Lin, T. Ocheltree, M. Vialpando, A. Kacuba, R. Justice, R. Pazdur, Folutyn (pralatrexate injection) for the treatment of patients with relapsed or refractory peripheral T-cell lymphoma: U.S. Food and Drug Administration drug approval summary, *Clin. Cancer Res.* 16 (2010) 4921–4927.
- [12] J.M. Zain, E. Marchi, Pralatrexate – from bench to bedside, *Drugs Today (Barc)* 46 (2010) 91–99.
- [13] S. Chattopadhyay, R.G. Moran, I.D. Goldman, Pemetrexed: biochemical and cellular pharmacology, mechanisms, and clinical applications, *Mol. Cancer Ther.* 6 (2007) 404–417.
- [14] A. Avallone, E.D. Gennaro, L. Silvestro, V.R. Iaffaioli, A. Budillon, Targeting thymidylate synthase in colorectal cancer: critical re-evaluation and emerging therapeutic role of raltitrexed, *Expert Opin. Drug Saf.* 13 (2014) 113–129.
- [15] M. Welin, J.G. Grossmann, S. Flodin, T. Nyman, P. Stenmark, L. Tresaugues, T. Kotenyova, I. Johansson, P. Nordlund, L. Lehtio, Structural studies of trifunctional human GART, *Nucleic Acids Res.* 38 (2010) 7308–7319.
- [16] J.E. Baggott, T. Tamura, Folate-dependent purine nucleotide biosynthesis in humans, *Adv. Nutr.* 6 (2015) 564–571.
- [17] J.E. Baggott, T. Tamura, Evidence for the hypothesis that 10-formyldihydrofolate is the in vivo substrate for aminoimidazolecarboxamide ribotide transformylase, *Exp. Biol. Med.* (Maywood) 235 (2010) 271–277.
- [18] E.C. Taylor, P.J. Harrington, S.R. Fletcher, G.P. Beardsley, R.G. Moran, Synthesis of the antileukemic agents 5,10-dideazaaminopterin and 5,10-dideaza-5,6,7,8-tetrahydroaminopterin, *J. Med. Chem.* 28 (1985) 914–921.
- [19] R.G. Moran, S.W. Baldwin, E.C. Taylor, C. Shih, The 6S- and 6R-diastereomers of 5, 10-dideaza-5, 6, 7, 8-tetrahydrofolate are equiactive inhibitors of de novo purine synthesis, *J. Biol. Chem.* 264 (1989) 21047–21051.
- [20] C.-G. Cheong, D.W. Wolan, S.E. Greasley, P.A. Horton, G.P. Beardsley, I.A. Wilson, Crystal structures of human bifunctional enzyme aminoimidazole-4-carboxamide ribonucleotide transformylase/IMP cyclohydrolase in complex with potent sulfonyl-containing antifolates, *J. Biol. Chem.* 279 (2004) 18034–18045.
- [21] A.C. Racanelli, S.B. Rothbart, C.L. Heyer, R.G. Moran, Therapeutics by cytotoxic metabolite accumulation: pemetrexed causes ZMP accumulation, AMPK activation, and mammalian target of rapamycin inhibition, *Cancer Res.* 69 (2009) 5467–5474.
- [22] S.B. Rothbart, A.C. Racanelli, R.G. Moran, Pemetrexed indirectly activates the metabolic kinase AMPK in human carcinomas, *Cancer Res.* 70 (2010) 10299–10309.
- [23] Y. Liu, C. Zhang, H. Zhang, M. Li, J. Yuan, Y. Zhang, J. Zhou, H. Guo, L. Zhao, Y. Du, L. Wang, L. Ren, Synthesis and antitumor activity of a novel series of 6-substituted pyrrolo[2,3-d]pyrimidines as potential nonclassical antifolates targeting both thymidylate and purine nucleotide biosynthesis, *Eur. J. Med. Chem.* 93 (2015) 142–155.
- [24] Y. Liu, M. Li, H. Zhang, J. Yuan, C. Zhang, K. Zhang, H. Guo, L. Zhao, Y. Du, L. Wang, L. Ren, Design, synthesis and biological evaluation of 6-substituted pyrrolo[2,3-d]pyrimidines as dual inhibitors of TS and AICARFTase and as potential antitumor agents, *Eur. J. Med. Chem.* 115 (2016) 245–256.
- [25] S. Raz, M. Stark, Y.G. Assaraf, Folylpolypoly- γ -glutamyl synthetase: a key determinant of folate homeostasis and antifolate resistance in cancer, *Drug Resist. Updat.* 28 (2016) 43–64.
- [26] E.G. Gibson, M.M. King, S.L. Mercer, J.E. Deweese, Two-mechanism model for the interaction of etoposide quinone with topoisomerase II α , *Chem. Res. Toxicol.* 29 (2016) 1541–1548.
- [27] A. Buqué, J.S. Muhialdin, A. Muñoz, B. Calvo, S. Carrera, U. Aresti, A. Sancho, I. Rubio, G. López-Vivanco, Molecular mechanism implicated in Pemetrexed-induced apoptosis in human melanoma cells, *Mol. Cancer* 11 (2012) 25.
- [28] S. McNicholas, E. Potterton, K.S. Wilson, M.E. Noble, Presenting your structures: the CCP4mg molecular-graphics software, *Acta Crystallogr. D. Biol. Crystallogr.* 67 (2011) 386–394.